

# On the Temperature Compensation of a Frequency Reference for Crystal-Less ULP Wireless Sensor Networks

Fabio Sebastiano\*, Lucien Breems\*, Kofi Makinwa<sup>†</sup> Salvatore Drago\*, Domine Leenaerts\* and Bram Nauta<sup>‡</sup>

\*NXP Semiconductors, Eindhoven, The Netherlands, Email: fabio.sebastiano@nxp.com

<sup>†</sup>Electronic Instrumentation Laboratory, Delft University of Technology, Delft, The Netherlands

<sup>‡</sup>IC Design Group, CTIT Research Institute, University of Twente, Enschede, The Netherlands

**Abstract**—Each node in a Wireless Sensor Network (WSN) must be provided with a frequency reference to enable network synchronization and RF communication. As the nodes need to be small, cheap and energy efficient, a frequency reference suitable for WSN must show low power consumption and require no off-chip components. A reference based on electron mobility in a MOS transistor demonstrates such features. Its output frequency follows the temperature dependence of mobility, which, although large, is well defined and can be compensated for. It is shown that a temperature sensor with accuracy of only 0.6 °C can be employed for the temperature compensation and that the inaccuracy of a compensated mobility-based frequency reference due to temperature, process spread, voltage supply variations and noise can be as low as 1% on a wide temperature range, fitting radio architectures for WSN applications.

## I. INTRODUCTION

Wireless Sensors Networks (WSN) are networks consisting of thousands of ubiquitous nodes, which are able to collect and share environmental parameters (such as temperature, pressure, vibrations, ...). Economical and physical requirements should be met to enable the deployment of such networks: each node is strongly constrained in terms of cost, size and power [1]. Regarding power consumption, the largest fraction of the energy consumed in each node is spent in the radio receiver in idle listening to the channel. The idle listening time and, consequently, the power consumption can be reduced if a synchronous network protocol is employed [2]. In that case, each node must be equipped with a time reference, which enables the prediction of the timeslot during which the reception of some data is expected. The receiver can then be turned on only during such timeslot. Thus, the energy saving is directly related to the accuracy of the timeslot prediction and, hence, to the accuracy of the time reference. Requirements on time/frequency accuracy are also present in the RF front-end. While commercial communication systems require high frequency accuracy, radios for WSN can be optimized to relax such specifications and so accuracies of only few percent are needed [2] [3].

To reduce both cost and size of the node, the common time/frequency references based on crystal oscillators can not be employed and fully-integrated solutions must be adopted. Though the same high accuracy of crystal oscillator is desirable, both to reduce power consumption and ease the RF

front-end design, accuracy must be given up for the sake of integration and accuracy in the order of few percents is acceptable [2]. In addition, the available power is limited to few tens of  $\mu\text{W}$ , since the time reference is turned on continuously, and the supply voltage must be kept low to be compliant with typical WSN energy sources, such as batteries and energy scavengers [4].

Recently, much work has been devoted to implementing fully integrated frequency references in standard microelectronic technologies. *LC* oscillators [5] can provide accuracy and phase noise performances comparable to XCOs; however, it is impracticable to reduce their power consumption below 100  $\mu\text{W}$  due to limited Q of integrated inductors and the possible need for high-speed frequency dividers. The accuracy of the compensated ring oscillator in [6] is high enough for WSN applications, but its power consumption is in the mW range. A very stable physical effect, i.e. the thermal diffusivity of bulk silicon, could be exploited for use in frequency references [7]; however, the silicon substrate needs to be heated to measure the diffusivity and this requires a few mW. The trimmed RC oscillator described in [8] also seems to achieve performances suitable for WSN, although the effect of process spread is not discussed.

An alternative way of realizing an accurate fully integrated oscillator is by employing charge mobility as a reference [9]. Mobility is less sensitive to process variations than other parameters, such as polysilicon resistance or oxide capacitance, and its standard deviation is less than 2% at room temperature for the adopted process. Although the temperature dependence of the mobility is large (approximately  $T^{-1.5}$ ), it is well defined and can be compensated for. The effect of process spread can then be removed by a single room temperature calibration.

This paper presents a proof of concept of a fully integrated oscillator referenced to the mobility, which is especially suited for use as a timing reference in a WSN. The oscillator is based on a current-controlled relaxation oscillator, in which the current is proportional to the mobility. Experimental validation of such approach will be provided, demonstrating a frequency spread in the temperature range of interest of less than 1.1% after one-point calibration and a power consumption of 41  $\mu\text{W}$ . The circuit is presented in section II; experimental results and

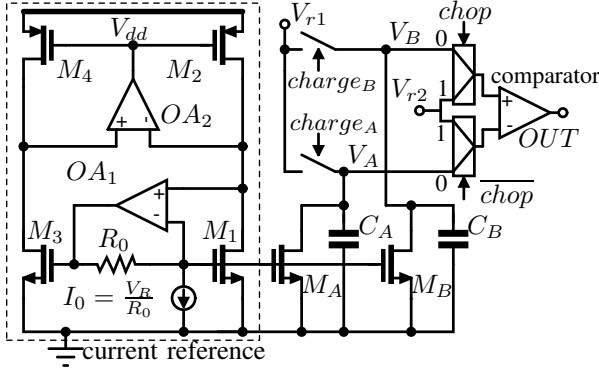


Fig. 1. Mobility-referenced oscillator.

an analysis of temperature compensation schemes are shown respectively in section III and IV and conclusions are drawn in section V.

## II. CIRCUIT DESCRIPTION

A simplified schematic of the oscillator is shown in Fig. 1. It consists of a current reference, two current mirrors  $M_1 - M_A$  and  $M_1 - M_B$ , two capacitors  $C_A$  and  $C_B$  and a comparator. The operation of the current reference, i.e. the circuit in the dashed box in Fig. 1, can be understood by noting that  $M_2$ ,  $M_4$  and  $OA_2$  constitute a low-voltage current mirror and that  $M_1$  is effectively diode-connected through  $OA_1$  and  $R$ . The current  $I_0$  is obtained from an external voltage  $V_R$  and an on chip resistor matching with  $R_0$ . Using the square-law MOS model, it is possible to derive [10]

$$I_1 = \frac{\mu_n C_{ox}}{2} \frac{W_1}{L_1} \frac{V_R^2}{\left(\sqrt{\frac{n}{m}} - 1\right)^2} \quad (1)$$

where  $\mu_n$  is the electron mobility,  $C_{ox}$  the gate capacitance per unit area,  $n = \frac{W_4/L_4}{W_2/L_2}$  and  $m = \frac{W_3/L_3}{W_1/L_1}$ . Additional components that were not essential to understand circuit operation, such as compensation capacitors or the start-up circuit, have been omitted in Fig. 1. More details about the implementation of the current reference and the comparator can be found in [11].

The drain current of  $M_1$  is mirrored by  $M_A$  and  $M_B$  with a gain of four and is given by

$$I_1 = \frac{I_A}{4} = \frac{I_B}{4} = \frac{\mu_n C_{ox}}{2} \frac{W_1}{L_1} k V_R^2 \quad (2)$$

where  $k$  a constant determined by ratios of matched transistors sizes. As shown in the timing diagram in Fig. 2,  $C_A$  and  $C_B$  are alternatively precharged to  $V_{r1}$  and then linearly discharged by  $M_A$  and  $M_B$ . When the voltage on the discharging capacitor drops below  $V_{r2}$ , the output of the comparator switches and the linear discharge of the other capacitor starts immediately, while the recharge is delayed by  $D$ . The delay  $D$  ensures that non-idealities of the comparator do not affect the slope of the discharge at the crossing of  $V_{r2}$  and it is not critical, as it does not influence the period  $T$ . The delay  $D$  and the

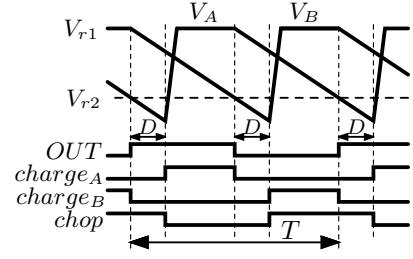


Fig. 2. Oscillator waveforms.

signals driving the switches are generated by a digital circuit not shown in Fig. 1.

By inspecting Fig. 1 and Fig. 2, the period and frequency of oscillation can be easily determined, and from (2):

$$T = \frac{2C}{I_A} (V_{r1} - V_{r2}) \Rightarrow f = \frac{1}{T} = \mu_n k \frac{C_{ox} W_1}{C} \frac{V_R^2}{V_{r1} - V_{r2}} \quad (3)$$

where  $C = C_A = C_B$ .  $C_A$  and  $C_B$  are implemented with MOS capacitors operated in inversion and matched with transistor  $M_1$ , in order to obtain a process and temperature independent ratio  $\frac{C_{ox} W_1}{C}$ . If the reference voltages  $V_{r1}$  and  $V_{r2}$  are obtained from a bandgap reference, the residual frequency variations will be due to the spread and temperature dependence of the mobility and the voltage  $V_R$ . The latter can be used as a control voltage to compensate for the effects of temperature variations and process spread.

The two multiplexers at the input of the comparator are driven by the signal *chop*, shown in Fig. 2, to mitigate the effect of comparator offset. Thus, with an offset  $V_{os}$  at the comparator input, the output is switched when  $V_A = V_{r2} - V_{os}$  or  $V_B = V_{r2} + V_{os}$  and the total error in the period is given by

$$\frac{\Delta t}{T} \cong \frac{V_{os}}{2(V_{r1} - V_{r2})} \left( \frac{\Delta C}{C} - \frac{\Delta I}{I_A} \right) \quad (4)$$

where  $\Delta C = C_A - C_B$  and  $\Delta I = I_A - I_B$ . Hence, if the capacitors and current mirrors are well matched, the resulting error is small. Since those components work at low frequency, good matching can be obtained by increasing device area and without significantly affecting oscillator's performances.

## III. EXPERIMENTAL RESULTS

The oscillator has been realized in a baseline TSMC 65-nm CMOS process. The circuit occupies 0.11 mm<sup>2</sup> and uses only 2.5-V I/O thick oxide MOS devices. 1.2-V thin oxide devices were avoided because of their high gate current, which is not negligible in very low current circuits. Most of the area of the circuit is occupied by the current reference and by the oscillator capacitors<sup>1</sup> (Fig. 3). For flexibility in testing, all the reference voltages ( $V_{ref1}$ ,  $V_{ref2}$ ,  $V_R$ ) were provided externally. For a nominal oscillation frequency of approximately 100 kHz, the reference current is  $I_1 = 125$  nA

<sup>1</sup>The area labeled as "capacitors" in Fig. 3 contains also transistors  $M_1$  and  $M_3$  of the current reference, which are required to match with MOS capacitor  $C_A$  and  $C_B$ .

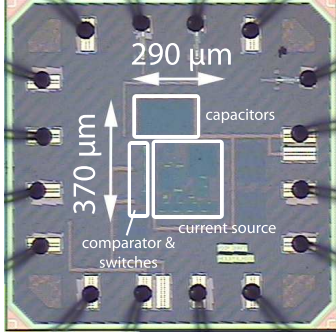


Fig. 3. Die micrograph of the test chip.

for  $C \cong 6$  pF,  $V_R = 0.2$  V,  $V_{ref1} = 1$  V and  $V_{ref2} = 0.6$  V. A low frequency was chosen to reduce the impact of parasitic effects, such as comparator delay. The total current consumption with 1.2 V supply voltage is  $34.3 \mu\text{A}$  ( $18.9 \mu\text{A}$  for comparator ad logic;  $14.4 \mu\text{A}$  for current reference;  $1 \mu\text{A}$  through pin  $V_{r1}$ ).

Frequency pushing is shown in Fig. 4. The nominal supply voltage of the circuit should be 2.5 V (with pMOS and nMOS threshold voltages of 0.63 V and 0.57 V respectively) but the chosen topologies of the current reference and comparator allow functionality down to 1.05 V. The upper bound of the supply voltage is limited to 1.39 V by the start-up circuit in the current reference. With reference to Fig. 4,  $V_{dda}$  supplies the current reference, while  $V_{ddd}$  supplies the logic and the comparator. The increase of frequency with  $V_{ddd}$  is due to a lower delay of the comparator for a higher voltage supply.

Long-term jitter measurements are reported in Fig. 5, together with lines showing the extrapolated thermal and flicker noise components. Period jitter is 52 ns (rms) and is dominated by comparator thermal noise. After a large number of periods, jitter is dominated by flicker noise from the current reference. Relative jitter is defined as the standard deviation of jitter divided by elapsed time; its value for a time period of the order of 1 s is an important parameter for time references used in WSN, since it limits duty-cycle of the receiver when synchronization is performed over a time scale of seconds [2]. It can be proven that for most oscillators, relative jitter becomes flat for increasing time, as observed in the measurements. The relative jitter is 0.1% after 1 s and is negligible compared to the temperature-induced frequency drift.

The temperature dependence of the output frequency is shown in Fig. 6. The measured average frequency is obtained from measurements on 11 samples from one batch trimmed at room temperature ( $22^\circ\text{C}$ ) and are in good accordance with simulations. The spread of the same samples with respect to the average frequency shown in Fig. 6 is below 1.1% ( $3\sigma$ ) over the range from  $-22^\circ\text{C}$  to  $85^\circ\text{C}$  after one-point calibration at  $22^\circ\text{C}$  (Fig. 7). For these measurements only, capacitors  $C_A$  and  $C_B$  were biased in deep inversion ( $V_{ddd} = 1.5$  V,  $V_{r1} = 1.6$  V,  $V_{r2} = 1.2$  V) to ensure that the spread is only due to the core circuit.

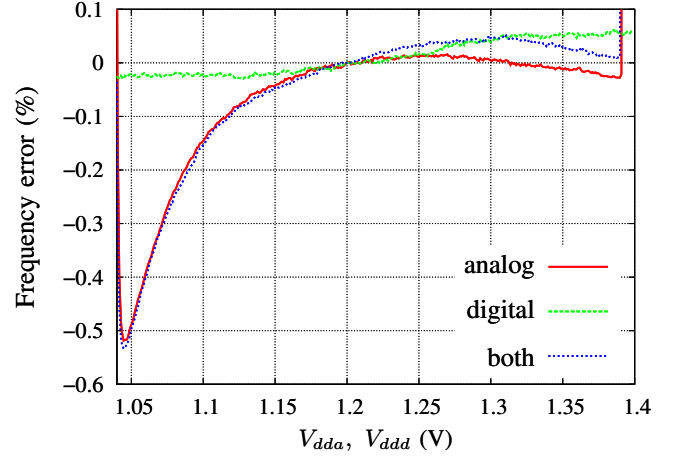


Fig. 4. Frequency error vs. variations of analog supply ( $V_{dda}$ ), digital supply ( $V_{ddd}$ ) or both.

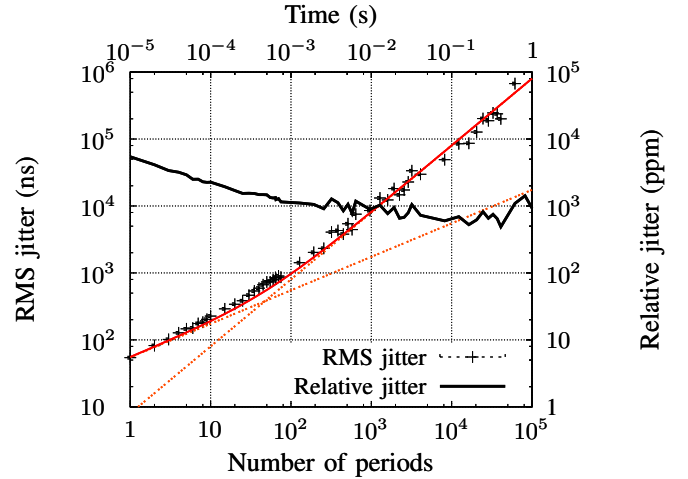


Fig. 5. Measured long-term jitter vs. time.

#### IV. TEMPERATURE COMPENSATION

Knowing the temperature dependence of the output frequency (Fig. 6), a compensation scheme can be applied. The compensation can be performed by varying a physical parameter in the oscillator circuit (Fig. 1), such as the voltage  $V_R$ , the gain of the current mirrors  $M_1 - M_A$  and  $M_1 - M_B$ , the capacitance  $C_A$  and  $C_B$ . Alternatively, compensation can be introduced in the processing of the output frequency, as for example varying the multiplication factor of a cascaded frequency multiplier or, if an alarm signal after a fixed time period is needed, changing the number of reference periods to be counted in the fixed period. Independently by the adopted scheme, the compensation parameter should be varied as a function of the temperature and an error in the measurement of the temperature would add additional spread on top of the spread shown in Fig. 7.

If the frequency is approximated as  $f = f_0 T^\alpha$  in a limited temperature range, an error in the measurement of temperature would cause a relative error in the compensated frequency

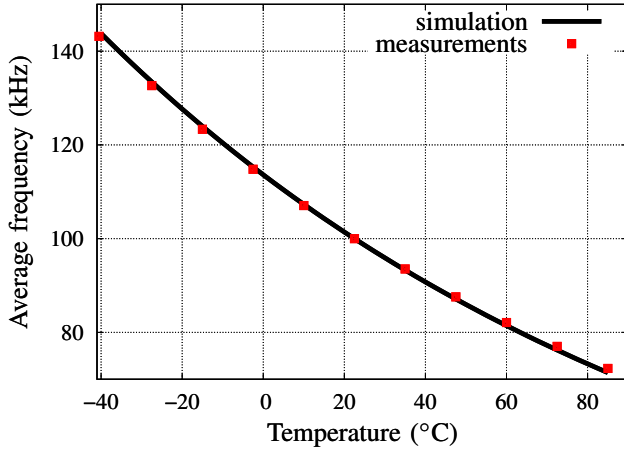


Fig. 6. Average output frequency (simulations and average on 11 measured samples) vs. temperature.

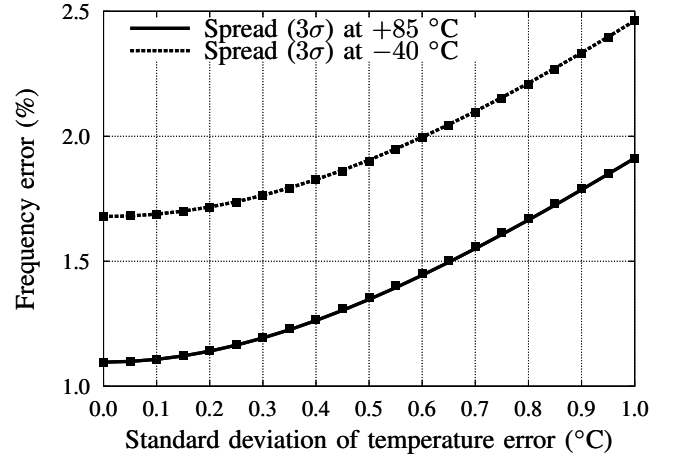


Fig. 8. Spread of the error of the compensated frequency vs. the standard deviation of the error in temperature estimation; simulation results and computation of Eq. (5) are plotted respectively with lines and squares.

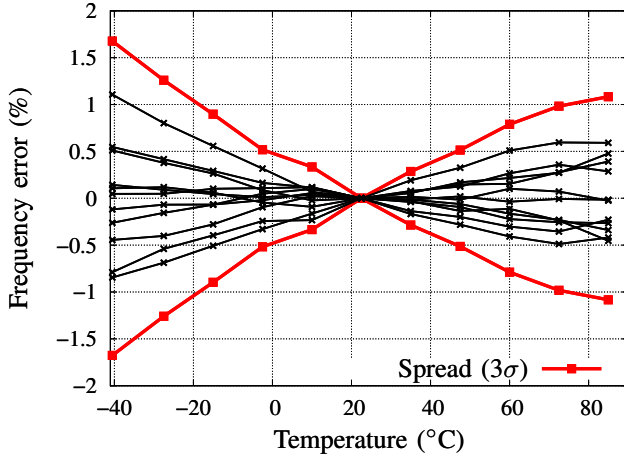


Fig. 7. Frequency error with respect to average frequency vs. temperature after one-point trimming at room temperature with  $V_R = 0.25$  V for 11 samples.

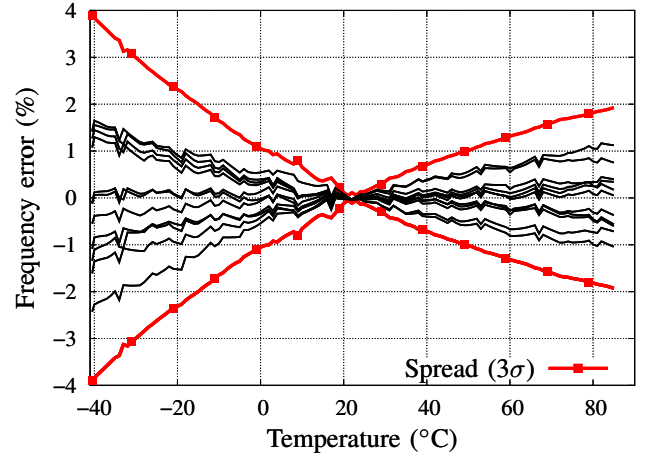


Fig. 9. Frequency error with respect to average frequency vs. temperature after one-point trimming at room temperature with  $V_R$  proportional to absolute temperature (PTAT).

given by

$$\sigma_{\frac{\Delta f}{f}} \approx \sqrt{\sigma_0^2 + \alpha^2 \sigma_{\frac{\Delta T}{T}}} \quad (5)$$

where  $\sigma_{\frac{\Delta f}{f}}$  is the standard deviation of the error in the compensated frequency,  $\sigma_0$  is the standard deviation of the error of the uncompensated frequency (i.e. the one reported in Fig. 7) and  $\sigma_{\frac{\Delta T}{T}}$  is the standard deviation of the relative error in the temperature measurement. Simulations have been performed, assuming an ideal compensation by a multiplicative factor and a random error in temperature measurement, and results are reported in Fig. 8. Eq. (5) is also plotted in the figure using for  $\alpha$  values extracted from the data in Fig. 6, i.e.  $\alpha = 1.4$  for  $T = -40$  °C and  $\alpha = 1.9$  for  $T = 85$  °C. A degradation of the spread less than 5% is observed at both corners of the temperature range for an error of 0.2 °C. Such accuracy can be easily reached with integrated temperature sensors and power

consumption<sup>2</sup> of the order of some tens of  $\mu$ W [12].

A lower sensitivity to temperature errors can be obtained if  $\alpha$  in (5) is decreased. That can be achieved using for  $V_R$  a temperature-dependent voltage instead of a temperature-independent one, as it has been done for the measurement shown in Fig. 7. A particular case is the use of a  $V_R$  proportional to the absolute temperature (PTAT). This would be advantageous also in terms of implementation, as bandgap voltage references, which are commonly employed to generate a temperature-independent voltage, requires to internally generate a PTAT voltage [13] [14]. The use of a PTAT  $V_R$  would result in  $\alpha \approx 0.5$  (with reference to Eq. (3)) and, consequently, to a smaller spread for a fixed accuracy of the temperature sensor. A PTAT  $V_R$  has been applied to the

<sup>2</sup>Further decrease in power consumption can be achieved duty-cycling the temperature sensor, since temperature variations are usually characterized by slow time constants and continuous sensing is not required.

test-chip and results are reported in Fig. 9. To reduce the measurement time, a fixed set of values of  $V_R$  have been applied to the circuit for different temperatures. Interpolation have been used to extrapolate the behavior of the circuit for any value of temperature and  $V_R$  and the compensation have been performed off-line for each of the 11 samples on the extrapolated data. The interpolation is then the cause of the disturbances visible in the figure. The application of a PTAT  $V_R$  increases the spread with respect to the constant  $V_R$  case (i.e. Fig. 7). Note that the compensation has been performed without adding any error in the temperature measurement. The larger spread can be explained analyzing the effect of threshold voltage mismatch between transistors  $M_1$  and  $M_2$  in Fig. 1. Taking into account a threshold voltage mismatch  $\Delta V_{th}$  between  $M_1$  and  $M_2$ , Eq. (2) is modified as

$$f(T) = \mu_n k \frac{C_{ox} \frac{W_1}{L_1}}{C} \frac{(V_R(T) + \Delta V_{th})^2}{V_{r1} - V_{r2}} \quad (6)$$

After trimming at temperature  $T_0$ , it can be easily proven that the frequency error due to the threshold voltage mismatch is zero in the case of temperature-independent  $V_R$  and given by the following expression in the case of a PTAT  $V_R$ :

$$\frac{\Delta y}{y} \approx \frac{2\Delta V_{th}}{V_R(T_0)} \frac{T_0 - T}{T} \quad (7)$$

where  $y = \frac{f(T)}{f(T_0)}$  is proportional to the compensated frequency. It can then be concluded that better performances are achieved with compensation schemes which keep  $V_R$  temperature independent.

## V. CONCLUSIONS

A fully integrated mobility-based frequency reference has been presented. Its frequency inaccuracy, due respectively to temperature, supply variations and noise, amounts to 1.1% ( $3\sigma$ ) from  $-22^\circ\text{C}$  to  $85^\circ\text{C}$ , 0.1% with 0.24 V supply variation and 0.1% (rms) over 1 s time span. The employment of an integrated temperature sensor with accuracy of only  $0.6^\circ\text{C}$  ( $3\sigma$ ) for the temperature compensation scheme would not affect appreciably the accuracy of the frequency reference. This shows that mobility can be used to generate a reference frequency accurate enough for WSN applications and that the proposed architecture is both low-voltage and low-power, as required by autonomous sensor nodes.

## ACKNOWLEDGMENT

This work is funded by the European Commission in the Marie Curie project TRANSSAT - 2005-020461.

## REFERENCES

- [1] J. Ammer, F. Burghardt, E. Lin, B. Otis, R. Shah, M. Sheets, and J. M. Rabaey, "Ultra low-power integrated wireless nodes for sensor and actuator networks," in *Ambient Intelligence*, W. Weber, J. M. Rabaey, and E. Aarts, Eds. Springer, 2005.
- [2] F. Sebastiano, S. Drago, L. Breems, D. Leenaerts, K. Makinwa, and B. Nauta, "Impulse based scheme for crystal-less ULP radios," in *Proc. ISCAS*, May 2008, pp. 1508 – 1511.
- [3] N. M. Pletcher and S. Gambini, "A 2 GHz 52  $\mu\text{W}$  wake-up receiver with  $-72$  dBm sensitivity using uncertain-IF architecture," in *IEEE ISSCC Dig. of Tech. Papers*, Feb. 2008, pp. 524 – 525.

- [4] S. Chalasani and J. Conrad, "A survey of energy harvesting sources for embedded systems," *Southeastcon, 2008. IEEE*, pp. 442–447, April 2008.
- [5] M. S. McCorquodale, S. M. Pernia, J. D. O'Day, G. Carichner, E. Marsman, N. Nguyen, S. Kubba, S. Nguyen, J. Kuhn, and R. B. Brown, "A 0.5-to-480 MHz self-referenced CMOS clock generator with 90 ppm total frequency error and spread-spectrum capability," in *ISSCC Dig. of Tech. Papers*, Feb. 2008, pp. 524 – 525.
- [6] K. Sundaresan, P. Allen, and F. Ayazi, "Process and temperature compensation in a 7-MHz CMOS clock oscillator," *IEEE J. Solid-State Circuits*, vol. 41, no. 2, pp. 433–442, Feb. 2006.
- [7] C. Zhang and K. Makinwa, "Interface electronics for a CMOS electrothermal frequency-locked-loop," in *Proc. ESSCIRC*, Sept. 2007, pp. 292 – 295.
- [8] M. Paavola, M. Laiho, M. Saukoski, and K. Halonen, "A 3  $\mu\text{W}$ , 2 MHz CMOS frequency reference for capacitive sensor applications," in *Proc. ISCAS*, May 2006, pp. 4391–4394.
- [9] R. Blauschild, "An integrated time reference," *IEEE ISSCC Dig. of Tech. Papers*, pp. 56–57, 1994.
- [10] W. Sansen, F. Op't Eynde, and M. Steyaert, "A CMOS temperature-compensated current reference," *IEEE J. Solid-State Circuits*, vol. 23, no. 3, pp. 821–824, 1988.
- [11] F. Sebastiano, L. Breems, K. Makinwa, S. Drago, D. Leenaerts, and B. Nauta, "A low-voltage mobility-based frequency reference for crystal-less ULP radios," in *Proc. ESSCIRC*, Sept. 2008, pp. 306 – 309.
- [12] M. Pertjys, K. Makinwa, and J. Huijsing, "A cmos smart temperature sensor with a  $3\sigma$  inaccuracy of  $\pm 0.1^\circ\text{C}$  from  $-55^\circ\text{C}$  to  $125^\circ\text{C}$ ," *Solid-State Circuits, IEEE Journal of*, vol. 40, no. 12, pp. 2805–2815, Dec. 2005.
- [13] G. C. M. Meijer, "Concepts for bandgap references and voltage measurement systems," in *Analog circuit design: low-noise, low-power, low-voltage; mixed-mode design with CAD tools; voltage, current and time references*, J. H. Huijsing, R. J. van de Plassche, and W. M. C. Sansen, Eds. Norwell, MA, USA: Kluwer Academic Publishers, 1996, pp. 243–268.
- [14] B. Gilbert, "Monolithic voltage and current references: theme and variations," in *Analog circuit design: low-noise, low-power, low-voltage; mixed-mode design with CAD tools; voltage, current and time references*, J. H. Huijsing, R. J. van de Plassche, and W. M. C. Sansen, Eds. Norwell, MA, USA: Kluwer Academic Publishers, 1996, pp. 269–352.